Journal of Advanced Research in Applied Sciences and Engineering Technology

Journal homepage:
https://semarakilmu.com.my/journals/index.php/applied_sciences_eng_tech/index
ISSN: 2462-1943

Enhanced Polynomial Interpolation-Based SVPWM Control for A PMSG Horizontal Axis Wind Turbine under Varying Operating Conditions

Omar Stihi[1], Reda Dermouche[2], Boudjema Fares[1], Mohamed Tadjine[1], Nadjet Zioui[3,*]

[1] École Nationale Polytechnique, 10 Rue des Frères OUDEK, El Harrach 16200, Algiers, Algeria
[2] École Nationale Supérieure des Technologies Avancées, Bordj El Kiffan, Algiers, Algeria
[3] Université du Québec à Trois-Rivières, 3351 Bd des Forges, Trois-Rivières, QC G8Z 4M3, Canada

ARTICLE INFO

Article history:
Received 1 January 2026
Received in revised form 20 January 2026
Accepted 25 January 2026
Available online 23 February 2026

Keywords:

SVPWM; State feedback; Backstepping; Wind turbine; PMSG; Varying operating conditions

ABSTRACT

This study presents an improved control strategy for a 5.5 kW horizontal-axis wind turbine. The control schemes are initially developed using state-feedback and backstepping techniques, then improved using polynomial interpolation technique. The control objectives were defined according to distinct wind speed regions. The interpolation-based approach is proposed to determine the pitch angle variations as a function of wind speed, ensuring maximum power extraction even under abrupt wind fluctuations. A second interpolation is employed to compute optimal voltage references for different wind speeds, enabling fast and effective system response under rapidly varying wind conditions. These voltage references are implemented using space vector pulse width modulation (SVPWM), which is well known for its superior performance in terms of energy quality, noise reduction, and harmonic distortion, compared to other modulation techniques. The proposed control strategy mitigates power peaks and irregular transient behavior during transitions between operating regions. Unlike most of the works found in the literature, the proposed strategy is evaluated across all four operating zones rather than focusing only on maximum power point tracking (MPPT) or limiting the maximum extracted power. Additionally, wind gusts are incorporated into the simulation tests to reflect more realistic operating conditions. The simulation results demonstrate that the proposed approach effectively manages wind gusts and operating-zone transitions with stable and robust performances across all four regions.

1. Introduction

In recent years, wind turbines (WTs) have attracted increasing research interest, driven primarily by the pursuit of greater energy autonomy and the reduction of carbon emissions using clean energy sources [1-3]. Consequently, the development of improved WT designs and the enhancement of energy production using advanced control techniques remain active and timely research areas [4-6].

In a comparative analysis, Ramadan et al. (2025) introduced advanced control approaches aimed at improving wind turbine blade pitch systems [7]. Their study evaluated the harmony search algorithm and the exponential distribution optimizer for tuning PID controllers across a range of

* *Corresponding author.*
E-mail address: Nadjet.Zioui@uqtr.ca

operating conditions, demonstrating that the latter achieved superior performance, particularly in enhancing wind turbine operation under dynamic environmental conditions.

Other widely adopted control approaches include learning-based methods [8, 9], predictive model–based strategies [10, 11], and fractional-order control techniques [12- 15]. Another stream of research focuses on inertia- and frequency analysis–based methods aimed at reducing speed deviation magnitude and settling time in wind turbines, while ensuring coordination between mechanical load control and primary frequency control [16- 18]. Additional approaches involve probabilistic techniques for forecasting energy production or disturbances [19, 20]. Most control strategies rely on the blade or pitch angle as the primary control variable [21, 22], whereas a smaller number of studies employ the yaw angle for power control [23- 25]. Additionally, space vector pulse width modulation (SVPWM) continues to be one of the most widely used modulation strategies in power-electronics-based wind energy conversion systems (WECS), due to its efficient DC-bus utilization, reduced harmonic distortion, and ease of digital implementation [26- 30].

Despite significant progress, a clear research gap remains. Most existing studies rely on simulation-based validation using idealized or simplified wind-speed profiles. In addition, some reported results lack physical realism, such as inconsistencies in the signs of torque and power that imply the wind turbine operates as a power consumer rather than a generator. Furthermore, although an increasing number of studies in recent years have successfully implemented SVPWM, the majority focus primarily on optimal power point tracking or maximum power extraction configurations. In fact, only a limited number of studies have addressed WT control across all operating zones within a single framework. Even fewer have considered the impact of wind gusts in the speed profiles. Consequently, a promising research direction would be the development of a comprehensive control strategy that manages all operating zones with smooth and appropriate transitions. This approach should also be validated under realistic conditions, including scenarios with gusty wind profiles.

This study presents the design and implementation of an SVPWM-based backstepping state-feedback control scheme for a horizontal-axis wind turbine. The proposed approach is implemented and evaluated under realistic wind conditions, covering all operating regions. The test scenarios include diverse wind speed profiles that induce severe transients, as well as optimal and maximum operating conditions of the wind turbine. In contrast to previous studies, this work introduces an enhanced strategy based on polynomial interpolation to mitigate transient disturbances during transitions between operating regions and to improve robustness under gusty wind conditions.

The remainder of the document is organized as follows: Section 2 describes the tools and methods, including the WT model, SVPWM, state feedback, and backstepping techniques, along with the structure of the proposed control solution. Section 3 presents and analyzes the results, and Section 4 concludes the document, offering suggestions for future research directions.

2. Tools and methods

2.1 Wind turbine model

2.1.1 Aerodynamic model

Wind first flows through the blades of a horizontal axis wind turbine (HAWT), starting the energy conversion process. Blade element momentum theory (BEM) is often used to model rotor aerodynamics. BEM combines blade-element and momentum theories. The mechanical power P_w that the rotor captures is [31]:

$$P_w = \frac{1}{2}\rho A {v_w}^3 C_p(\lambda, \beta) \quad (1)$$

ρ is the air density
A is the area swept by the rotor ($A = \pi R^2$)
R is the rotor radius
v_w is the wind speed,
$C_p(\lambda, \beta)$ is the power coefficient that depends on the tip-speed ratio ($\lambda = \frac{\omega_{rt} R}{v_w}$) and the blade pitch angle β.
ω_{rt} is the angular speed of the rotor of the turbine.

The expression of the power coefficient $C_p(\lambda, \beta)$ is provided in equation (2) [32].

$$\begin{cases} C_p(\lambda, \beta) = c_1 \left(\frac{c_2}{\lambda_i} - c_3\beta - c_4\right) exp\left(-\frac{c_5}{\lambda_i}\right) + c_6\lambda \\ \lambda_i = \left(\frac{1}{\lambda + 0.08\beta} - \frac{0.035}{\beta^3 + 1}\right)^{-1} \end{cases} \quad (2)$$

c_1 to c_6 are constant parameters of the model.

The power extracted by the WT is constrained by the Betz limit to around 59.3% of the kinetic energy of the wind [33].

The mechanical torque T_m on the rotor shaft of the turbine is determined using the following expression:

$$T_m = \frac{P_w}{\omega_{rt}} \quad (3)$$

2.1.2 Mechanical transmission

In many systems, there is a mechanical transmission, between the turbine rotor and the generator, including a potential gearbox, that adapts the low-speed, high-torque output of the turbine rotor to the high speed required by the generator. This coupling is modeled so that the generator angular speed ω_{gen} is related to the turbine speed ω_{rt} by the gear ratio k_{gb} such as $k_{gb} = \frac{\omega_{gen}}{\omega_{rt}}$. Mechanical dynamics can be modeled by a mass-spring-damper system. Therefore, the mechanical model including the shaft and rotor can be modeled using the fundamental dynamics equation as the following [33]:

$$J\frac{d\omega_{rt}}{dt} = T_m - f\omega_{rt} - T_{el} \quad (4)$$

T_{el} is the electromagnetic torque.
f is the viscous friction coefficient of the rotor.
J is the total inertia that merges the WT and hub inertia J_{wt} and the electrical generator rotor with the shaft's inertia J_{gen}, such as $J = \frac{J_{wt}}{k_{gb}} + J_{gen}$.

2.1.3 Permanent Magnet Synchronous Generator (PMSG)

In the electrical part of the wind energy conversion system, the captured mechanical power is converted into electric power by a Permanent Magnet Synchronous Generator (PMSG). For modeling the PMSG, the standard approach is to use the synchronous-rotating reference $d - q$ frame to express the stator voltage and flux equations derived from the electrical scheme of the PMSG depicted in Figure 1. The stator voltage equations can be written as follows [34]:

$$\begin{cases} v_d = R_s i_d + L_s \frac{di_d}{dt} - L_s i_q p\omega_{wt} \\ v_q = R_s i_q + L_{sq} \frac{di_q}{dt} + L_s p\omega_{wt} i_d + \varphi_m p\omega_{wt} \end{cases} \quad (5)$$

v_d and v_q are the stator voltages in d and q axes, respectively
i_d and i_q are the stator currents, expressed in the q and q axes, respectively.
R_s is the stator resistance
φ_m is the flux due to permanent magnets
L_s is the inductance.

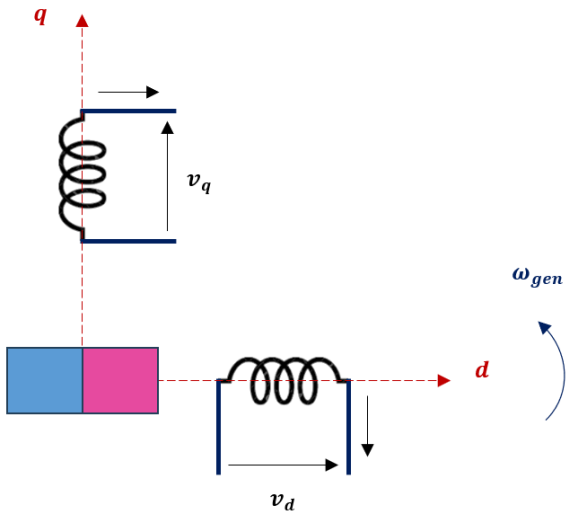

Fig. 1. The PMSG equivalent electrical scheme

From the voltages equations the electromagnetic torque's expression can be derived as follows:

$$T_{el} = \frac{3}{2} p \varphi_m i_q \quad (6)$$

p is the number of pole pairs.

In surface mounted PMSG machines, the inductances of the d and q axes are close, which simplifies the torque's expression to (6).

2.1.4 Power converter

To interface the PMSG with the grid, modern WECS often use a full-scale back-to-back (B2B) converter. A B2B converter typically consists of two three-phase voltage-source converters (VSCs) connected back-to-back, sharing a common DC-link with capacitor, as depicted in Figure 2. One of the converters, that is the machine side converter (MSC) is located on the generator side, the other, namely the grid converter side (GSC) is on the grid side [35].

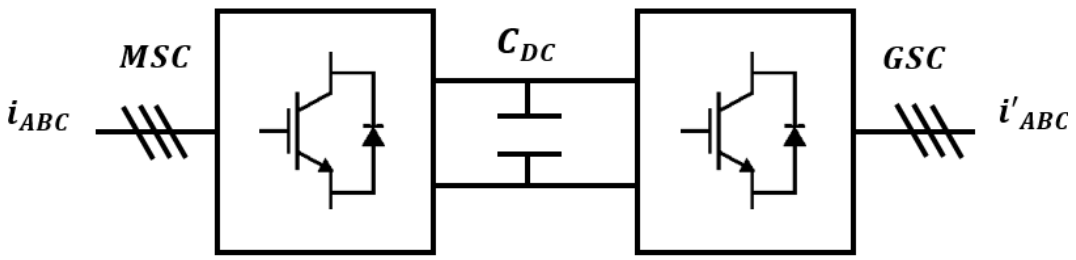

Fig. 2. Diagram of the B2B converter used in the PMSG based WT

The MSC is a rectifier. It converts the PMSG's three-phase AC output to DC, feeding the DC-link. The GSC converts from DC to three-phase AC under grid frequency, injecting power into the grid. This

decoupling via DC-link allows variable-speed operation of the PMSG while still delivering fixed-frequency AC to the grid [35].

The MSC then uses PWM switching signals to generate the required inverter voltages which represent the references for v_d and v_q. The MSC control often adjusts the generator rotor speed or the electromagnetic torque to match a given reference [35].

The GSC uses the DC-link voltage and injects three-phase AC to the grid. The control objectives are to regulate DC-link voltage, deliver active power to the grid, and manage reactive power [35].

Considering the switching functions S_1,..., S_6 for the MSC and S'_1,..., S'_6 for the GSC, $S_i = 1$ or $S'_1 = 1$ means the i^{th} switch is ON. Otherwise, the switch function's value is 0. The converter phase to neutral voltages v_{AN}, v_{BN}, v_{CN}, v'_{AN}, v'_{BN}, and v'_{CN} can be expressed as in relationships (7) and (8) for the MSC and GSC, respectfully [36].

$$\begin{pmatrix} v_{AN} \\ v_{BN} \\ v_{CN} \end{pmatrix} = \frac{V_{DC}}{3} \begin{pmatrix} 2S_1 - S_3 - S_5 \\ 2S_3 - S_1 - S_5 \\ 2S_5 - S_3 - S_1 \end{pmatrix} \quad (7)$$

$$\begin{pmatrix} v'_{AN} \\ v'_{BN} \\ v'_{CN} \end{pmatrix} = \frac{V_{DC}}{3} \begin{pmatrix} 2S'_1 - S'_3 - S'_5 \\ 2S'_3 - S'_1 - S'_5 \\ 2S'_5 - S'_3 - S'_1 \end{pmatrix} \quad (8)$$

Both MSC and GSC shar the DC capacitor. The model representing the dynamic of this DC-bus is as follows [35]:

$$\frac{dv_{DC}}{dt} = \frac{1}{C_{DC}}\left(i_{DCgen} - i_{DCgrid}\right) \quad (9)$$

i_{DCgen} and i_{DCgrid} are the DC currents from the MSC and GSC, respectfully. They can be computed using the phase currents of the MSC (i_A, i_b, and i_C) and the GSC (i'_A, i'_B, and i'_C) as the following:

$$\begin{cases} i_{DCgen} = S_1 i_A + S_3 i_B + S_5 i_C \\ i_{DCgrid} = S'_1 i'_A + S'_3 i'_B + S'_5 i'_C \end{cases} \quad (10)$$

In the following, the control of the DC link is supposed to be achieved, and the focus will be on the MSC side for power control.

2.2 Control method

2.2.1 Control objectives

The control of the WT depends on the wind speed which defines four operating zones:

- Zone 1 ($0 \leq V_w < 4m/s$): The WT is off service while keeping the pitch angle β at zero.
- Zone 2 ($4 \leq V_w < 12m/s$): The WT is on service while keeping the pitch angle β at zero. In this operating zone, the speed is controlled to meet the optimal tip speed ratio using the control signal v_q.
- Zone 3 ($12 \leq V_w < 25m/s$): The WT is on service while keeping the speed at its maximum value using the control signal v_q. The pitch angle β is used to keep the electrical power at its maximum value.
- Zone 4 ($V_w > 25m/s$): The WT is off service while keeping the pitch angle β to its maximum value to protect the mechanical structure of the turbine.

In the four zones, the d-component of the current is controlled to be zero for a maximum torque control strategy as the electromechanical torque depends on the q-component of the current.

For the studied WT, the expression of β in Zone 3 was determined empirically based on the measurement presented in Figure 3 that can be approximated by the following formulas.

$$\begin{cases} \beta = -0.9197\,{V_w}^2 + 24.6297\,V_w - 163.0055 & if\ 0 \le \beta \le 13 \\ \beta = 0.0080\,{V_w}^3 - 0.6012\,{V_w}^2 + 16.2524\,V_w - 125.5 & if\ 13 \le \beta \le 25 \end{cases} \quad (11)$$

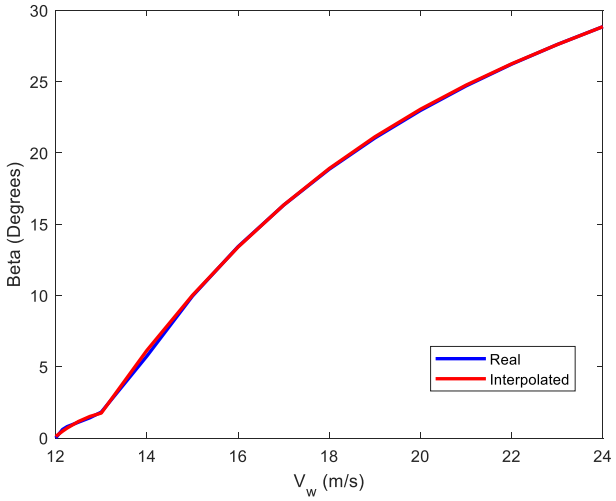

Fig. 3 The variations of the pitch angle with the wind speed in the third zone

Therefore, the control strategies developed in the following are valid for both second and third zones. Only the references and use of the pitch angle are different. Figure 4 illustrates the control objectives by operating zone.

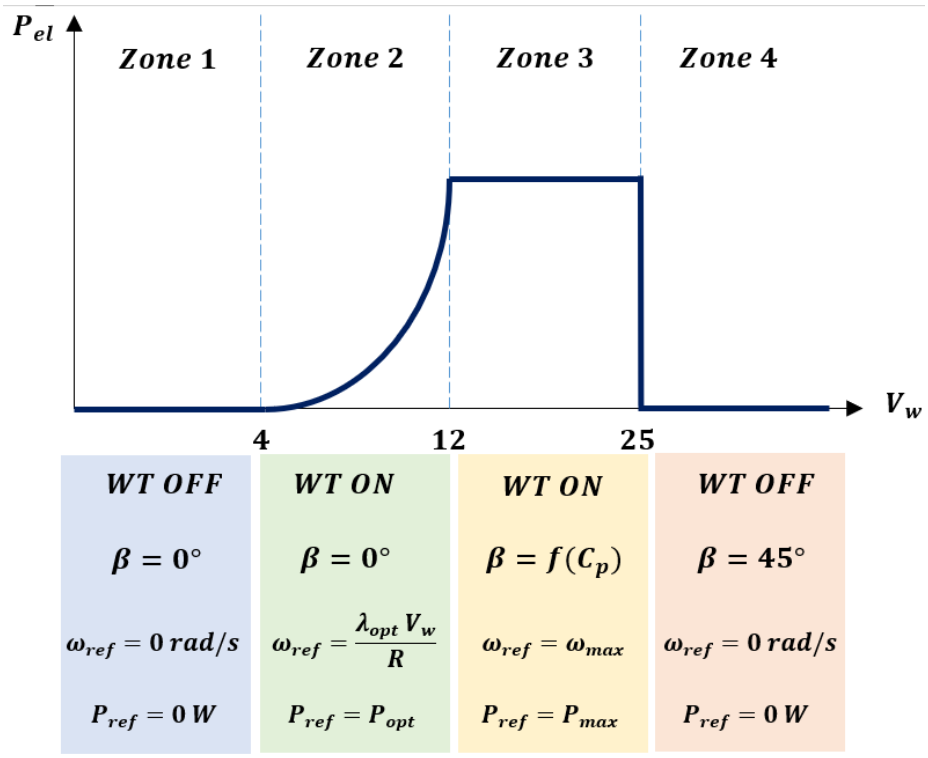

Fig. 4 The control objectives for each operating zone

2.2.1 State feedback control

State feedback control is based on the Lyapunov convergence criteria. Where a positive definite Lyapunov candidate function is defined such that the controller archives a negative definite derivative of this candidate function. The candidate function is usually based on the tracking errors of the state of the system, which requires rewriting equations (4) and (5) in terms of tracking errors as the following.

$$\begin{cases} \dot{e}_d = -\frac{R_s}{L_s} i_d + p\omega_{wt} i_q - \frac{di_{dr}}{dt} + \frac{1}{L_s} v_d \\ \dot{e}_q = -\frac{R_s}{L_s} i_q - p\omega_{wt} i_d - \frac{1}{L_s} p\varphi_m \omega_{wt} - \frac{di_{qr}}{dt} + \frac{1}{L_s} v_q \\ \dot{e}_\omega = \frac{1}{J}\left(\frac{3}{2} p\varphi_m i_q - T_m - f\omega_{wt}\right) - \frac{d\omega_{wtr}}{dt} \end{cases} \quad (12)$$

$e_d = i_d - i_{dr}$, $e_q = i_q - i_{qr}$, and $e_\omega = \omega_{wt} - \omega_{wtr}$ are the tracking errors for i_d, i_q, and ω_{wt} and i_{dr}, i_{qr}, and ω_{wtr} are the corresponding references.

2.2.3 Control of the d-component of the current

The application of the state feedback control to the d-component of the current of the PMSG considers the following Lyapunov positive definite function.

$$V_d = \frac{1}{2} {e_d}^2 \quad (13)$$

Its derivative is as follows:

$$\dot{V}_d = e_d \dot{e}_d = e_d \left(-\frac{R_s}{L_s} i_d + p\omega_{wt} i_q - \frac{di_{dr}}{dt} + \frac{1}{L_s} v_d\right) \quad (14)$$

The following control signal will ensure that $\dot{V}_d$ is negative definite:

$$v_d = R_s i_d - L_s p\omega_{wt} i_q + L_s \frac{di_{dr}}{dt} - L_s K_d e_d \quad (15)$$

K_d is a positive constant that determines the dynamic of convergence of the tracking error e_d to zero.

2.2.4 Backstepping control for the speed and q-component of the current

The backstepping controller is often used for multiple integrator-like systems. In the case of PMSG control, the approach uses i_q to control the speed ω_{wt} and the voltage v_q to control the current i_q. This goes through two steps:

Step 1: Use of i_q to control the speed ω_{wt}.

To achieve this first step of control, the following Lyapunov candidate function is defined:

$$V_\omega = \frac{1}{2} {e_\omega}^2 \quad (16)$$

Its derivative is as follows:

$$\dot{V}_\omega = e_\omega \dot{e}_\omega = e_\omega \left[\frac{1}{J}\left(\frac{3}{2} p\varphi_m i_q - T_m - f\omega_{wt}\right) - \frac{d\omega_{wtr}}{dt}\right] \quad (17)$$

The following reference for i_q will ensure that $\dot{V}_\omega$ is negative definite:

$$i_{qr} = \frac{2J}{3p\varphi_m}\left(T_m + f\omega_{wt} + J\frac{d\omega_{wtr}}{dt} - K_\omega e_\omega\right) \quad (18)$$

K_ω is positive constant that determines the dynamic of convergence of the tracking error e_ω to zero.

Step 2: Use of v_q to control the current component i_q.

To achieve this second step of control, the following Lyapunov candidate function is defined:

$$V_q = \frac{1}{2} {e_\omega}^2 + \frac{1}{2} {e_q}^2 \quad (19)$$

Its derivative is as follows:

$$\dot{V}_q = e_\omega \dot{e}_\omega + e_q \dot{e}_q$$
$$= e_\omega \left[\frac{1}{J}\left(\frac{3}{2}p\varphi_m i_q - T_m - f\omega_{wt}\right) - \frac{d\omega_{wtr}}{dt}\right] \quad (20)$$
$$+e_q\left(-\frac{R_s}{L_s}i_q - p\omega_{wt}i_d - \frac{1}{L_s}p\varphi_m\omega_{wt} - \frac{di_{qr}}{dt} + \frac{1}{L_s}v_q\right)$$

The following expression for v_q will ensure that $\dot{V}_q$ is negative definite:

$$v_q = R_s i_q + L_s p\omega_{wt} i_d + p\varphi_m\omega_{wt} + L_s\frac{di_{qr}}{dt} - \frac{L_s}{J}\frac{3}{2}p\varphi_m e_\omega - L_s K_q e_q \quad (21)$$

K_q is positive constant that determines the dynamic of convergence of the tracking error e_q to zero. This constant must be selected higher than K_ω so the error e_q converges faster than e_ω.

2.2.5 Proposed improvement of the control strategy

Due to transition issues, specifically between the first and second zones as well as the transition between zones 2 and 3, and improved controller is suggested in this section based on the empirical observation of the behavior of the WT in the second zone. This method is based on using the control strategy defined in the previous sections and defining the control signals formula based on the wind speed according to the desired objectives. A polynomial interpolation is then proposed to express the d and q voltages to smoothen the several curves while ensuring the tracking objectives Figures 5 depicts the v_d and v_q acquired voltages as well as the corresponding interpolated curves. The variations of v_q shows a straight-line curve that can be interpolated using a first order polynomial, whereas v_d shows a third order polynomial behavior. The two voltages can be represented by the following formulas.

$$\begin{cases} v_d = 0.0227\ {V_w}^3 + 0.0013\ {V_w}^2 - 0.0191\ V_w + 0.0432 \\ v_q = 16.0607\ V_w + 1.2663 \end{cases} \quad (22)$$

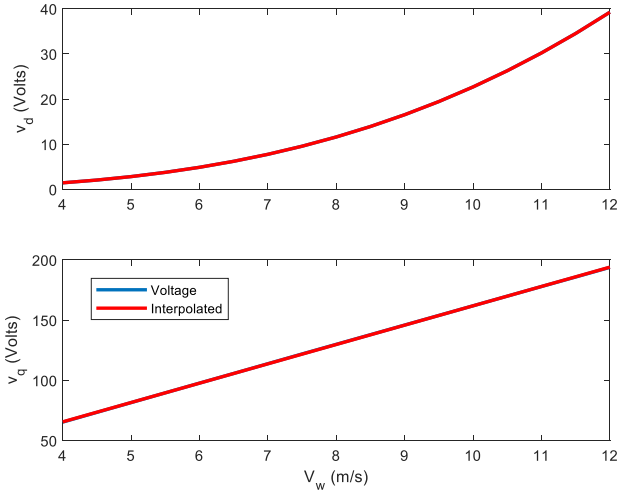

Fig. 5 Variations of the voltages with the wind speed

2.2.6 SVPWM

The implementation of the control strategy requires the use of a pulse width modulation (PWM) technique. Space vector pulse width modulation (SVPWM) is an advanced technique used to control the output voltage of a three-phase inverter where the goal is to create a three-phase AC voltage with a specific amplitude and frequency. The technique provides better voltage use and less harmonic distortion compared to traditional modulation techniques. It controls the switching of the

inverter's switches in such a way that it generates the desired output voltage waveform while minimizing the harmonic content [36].

The technique considers the space vector diagram of the inverter's output voltages. The space vector is a representation of the output voltage in a two-dimensional complex plane, where the voltage vectors are spaced 60° apart. The technique involves switching between different voltage vectors to generate the desired reference voltage [37].

The output of the three-phase inverter can be represented as a combination of 8 possible voltage vectors in the plane, with each vector corresponding to one of the 8 switching states of the inverter. These 8 voltage vectors are 6 active vectors (V1 to V6) that represent the voltages when two switches are ON, and one is OFF and vice versa, and 2 zero vectors (V0 and V7) that represent situations where all the upper or lower switches are simultaneously OFF or ON [37].

The space vector diagram results in a hexagon where the six active voltage vectors are positioned around the perimeter. The zero vectors are positioned at the center of the hexagon as depicted in Figure 3.

The three-phase voltages can be expressed in the $\alpha - \beta$ frame through the Clarke transform using the following relationship [36]:

$$\begin{pmatrix} v_\alpha \\ v_\beta \end{pmatrix} = \frac{2}{3}\begin{pmatrix} 1 & -1/2 & -1/2 \\ 0 & \sqrt{3}/2 & -\sqrt{3}/2 \end{pmatrix}\begin{pmatrix} v_{AN} \\ v_{BN} \\ v_{CN} \end{pmatrix} \quad (23)$$

The desired reference vector can be expressed as the following:

$$v_{ref} = \sqrt{{v_\alpha}^2 + {v_\beta}^2} \quad (24)$$

The module of the reference vector v_{ref} specifies the control of the output voltage waveform. With the value of the DC-bus voltage v_{DC}, it is also used to determine the modulation index m as in equation (25).

$$m = \frac{3}{2}\frac{v_{ref}}{v_{DC}} \quad (25)$$

Figure 6 illustrates the location of the reference voltage v_{ref} in the first sector of the $\alpha - \beta$ frame.

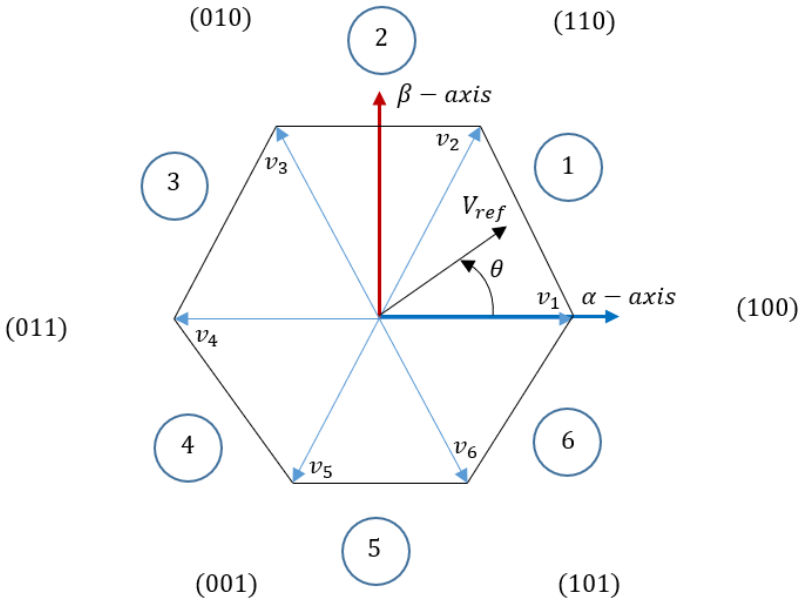

Fig. 6. Location of the reference in the space vector hexagon [36]

The reference voltage vector is decomposed into a combination of two adjacent active vectors and the duration of time each active vector needs to be applied. The reference vector lies between two of the active vectors in the space vector diagram, or sector. By calculating the time duration for each active vector and zero vector, the inverter switches in such a way that the resulting voltage approximates the reference.

The modulation strategy involves calculating how long each of the active and zero vectors should be applied. The two active vectors contribute to most of the reference voltage, and the zero vectors are used to balance the power and reduce harmonic distortion.

The switching times can be calculated geometrically by finding the time duration for each of the active vectors using the projection of the reference vector onto the adjacent active vectors in the space vector diagram. This will result in the following switching time formula [36]:

$$\begin{cases} T_1 = \sqrt{3}T_s \frac{V_{ref}}{U_{DC}} sin\left(\frac{\pi}{3} - \theta\right) \\ T_2 = \sqrt{3}T_s \frac{V_{ref}}{U_{DC}} sin\left(\theta - (n-1)\frac{\pi}{3}\right) \\ T_0 = T_s - (T_1 + T_2) \end{cases} \quad (26)$$

T_1 and T_2 are the times for the application of the first and second adjacent active vectors, respectfully. T_0 is the time of application of the zero vector and T_s is the switching period. The integer $n = 1, \dots, 6$ is the sector number and θ the angular position of v_{ref}.

3. Results and discussion

3.1. Simulation results

The simulations were carried out using MATLAB Simulink R2023b. Figure 7 illustrates the schematics of the program.

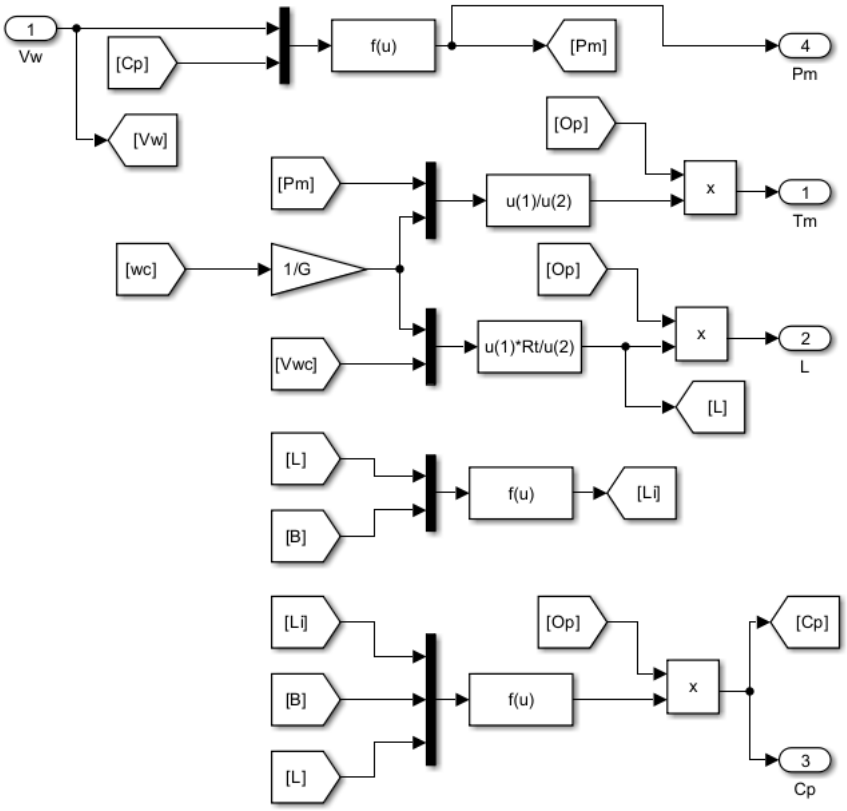

(a)

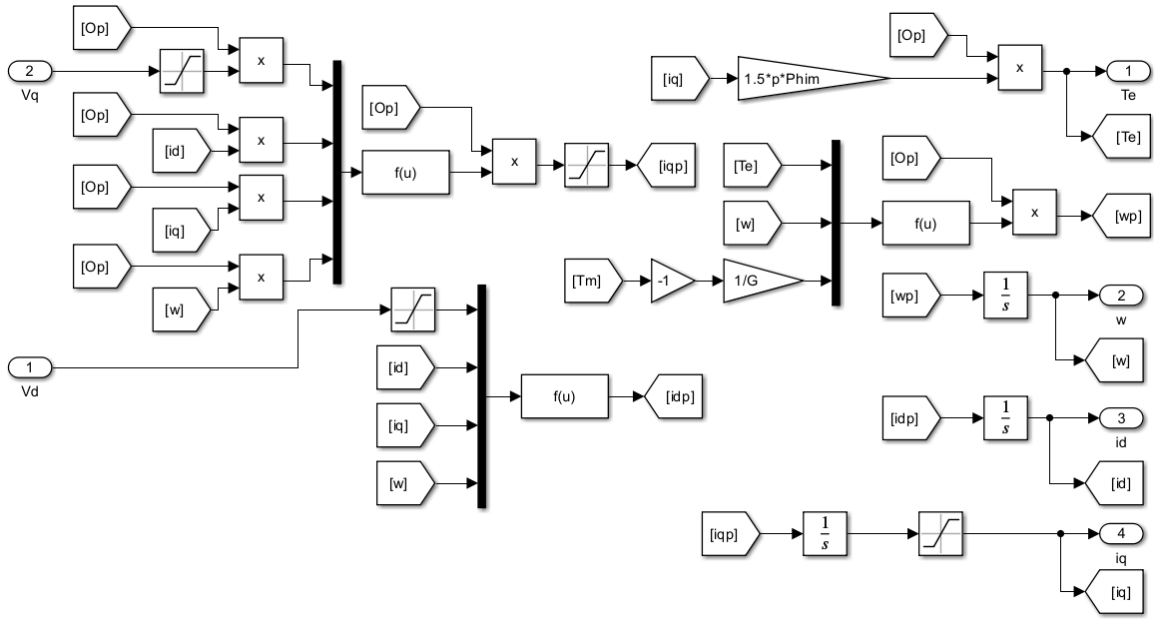
[Op]
2
Vq
[id]
[iq]
[w]
1
Vd
f(u)
[iqp]
[idp]
[Te]
[Tm]
-1
1/G
1.5*p*Phim
Te
[wp]
w
id
iq
[ed]
[eq]
[ew]
[idrp]
[vd23]
[vq23]
[Vw]
8.1*G*u/Rt
291.6
[wr1]
[wr2]
[wr3]
[wr4]
[idr]
[wr]
[wrp23]
[wrp14]
[iqr14]
[iqr23]
[iqrp23]
[iqrp14]

(b)

(c)

(d)

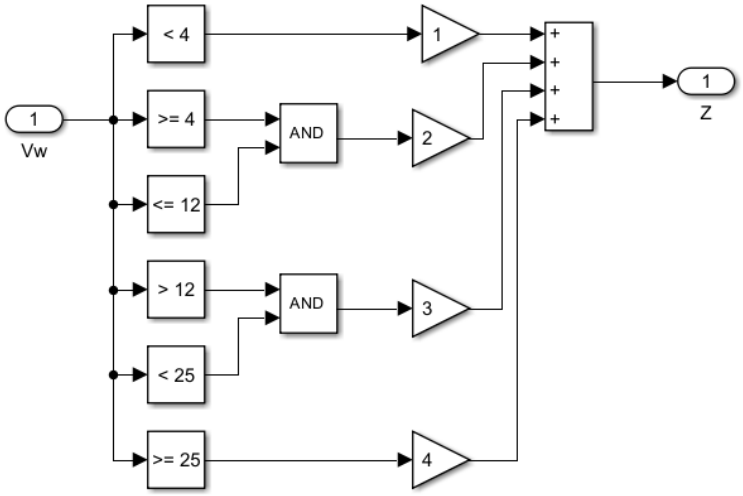

(e)

Fig. 7 The WT model and control strategy: (a) Aerodynamical model, (b) PMSG model, (c) The control signals, (d) The references, (e) The zone selection

The considered WT is rated 5.5 kW with maximum power of 6.5 kW. The parameters of the turbine are presented in Table 1 and the parameters of the PMSG in Table 2. The controller's parameters are $K_d = 10000$, $K_\omega = 30$, and $K_q = 10000$.

Table 1
The WT parameters

Parameter (unit)	Value
$\rho\ (kg/m^3)$	1.225
$R_t\ (m)$	2.5
λ_{opt}	8.1
C_{p_opt}	4.8
c_1	0.5176
c_2	116
c_3	0.4
c_4	5
c_5	21
c_6	0.0068

Table 2
The PMSG parameters.

Parameter (unit)	Value
$R_s\ (\Omega)$	0.0918
$Ls\ (H)$	0.001
$\varphi_m\ (V.s)$	0.1688
$J\ (kg.m^2)$	0.003945
$f\ (N.m.s)$	0.0004924
p	4
G	7.5

Figure 8 depicts the electrical power resulting from the wind speed profile presented in Figure 9. This wind speed profile has been chosen to cover the four operating zones of the WT.

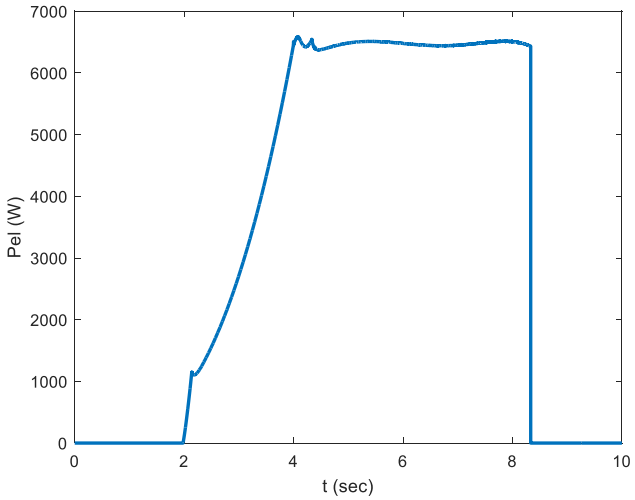

Fig. 8 Electrical power resulting from a ramp wind speed profile

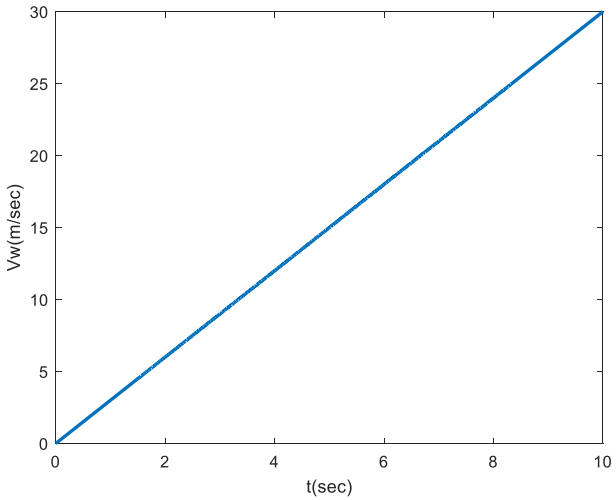

Fig. 9 Ramp wind speed profile

Figures 10 to 12 depict the currents, wind speed and the voltages profiles for the ramp test.

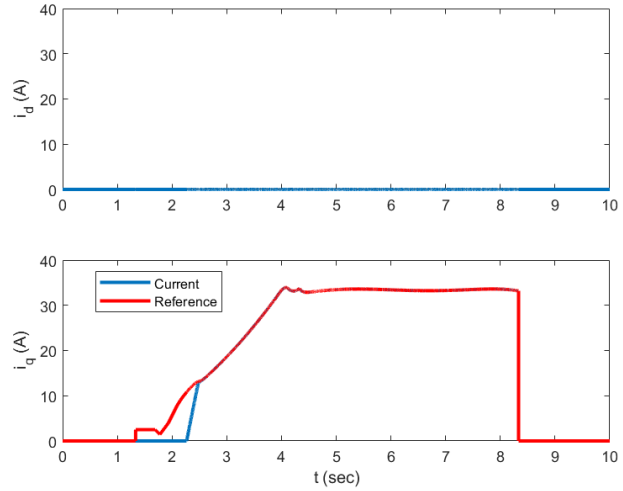

Fig. 10 The d and q components of the current

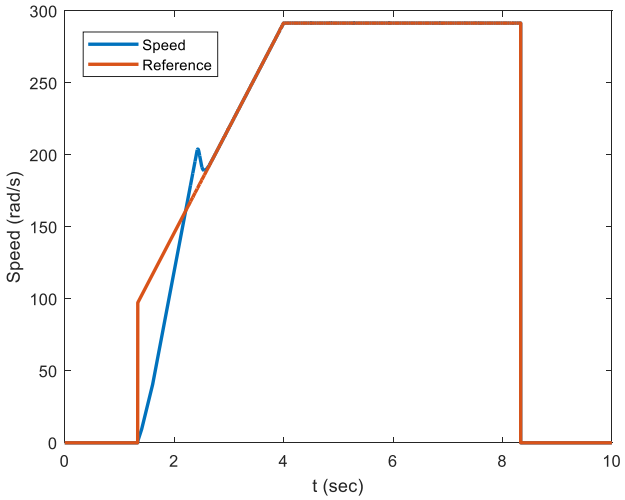

Fig. 11 Angular velocity results

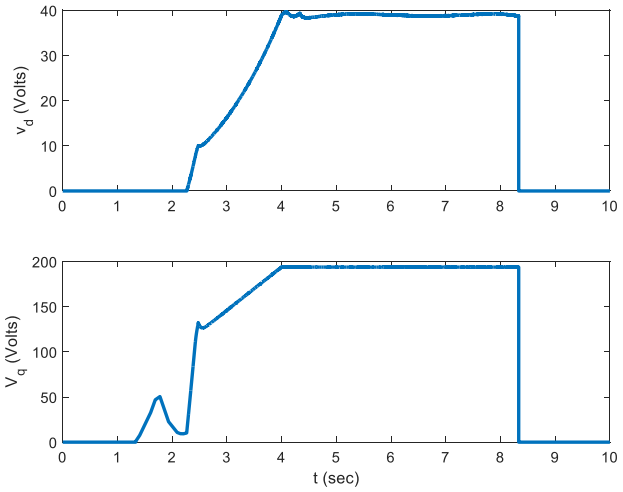

Fig. 12 The d and q voltages (control signals)

The improved strategy for the second zone resulted in the results presented in Figures 13 to 16 for the electrical power, currents, speed, and voltages, respectively.

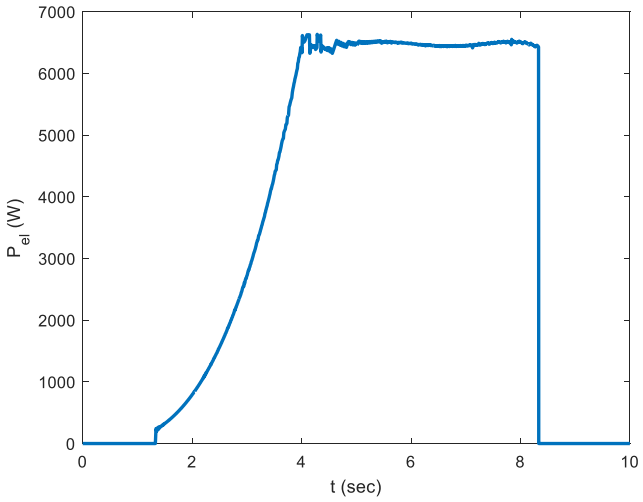

Fig. 13 Electrical power using the improved strategy

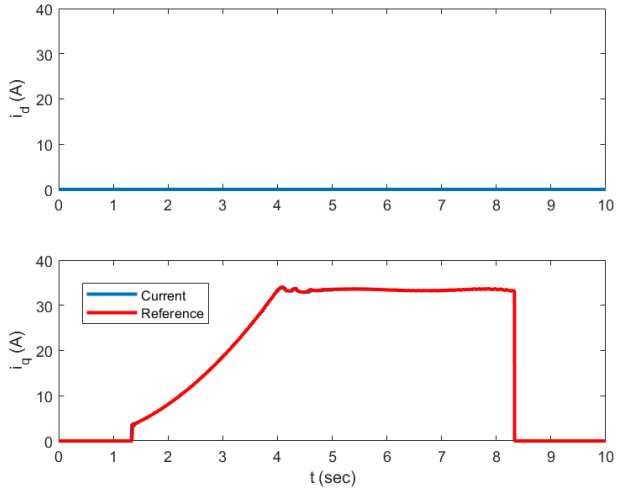

Fig. 14 The currents with the improved strategy

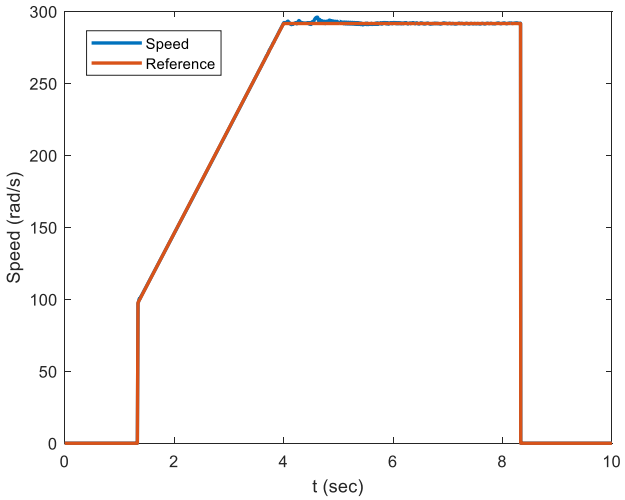

Fig. 15 The angular velocity with the improved strategy

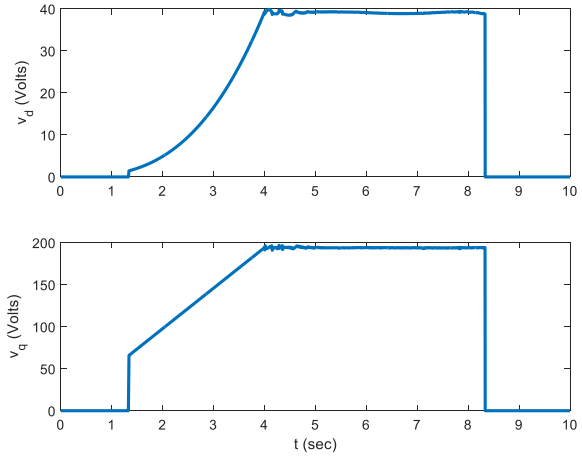

Fig. 16. The voltages using the improved strategy.

Figure 17 presents the power resulting from the presence of gusts in the wind speed profile depicted in Figure 18.

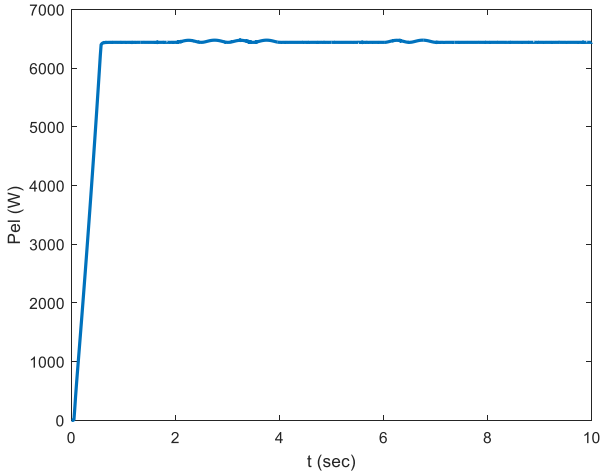

Fig. 17 The electrical power with gusts in the wind speed profile

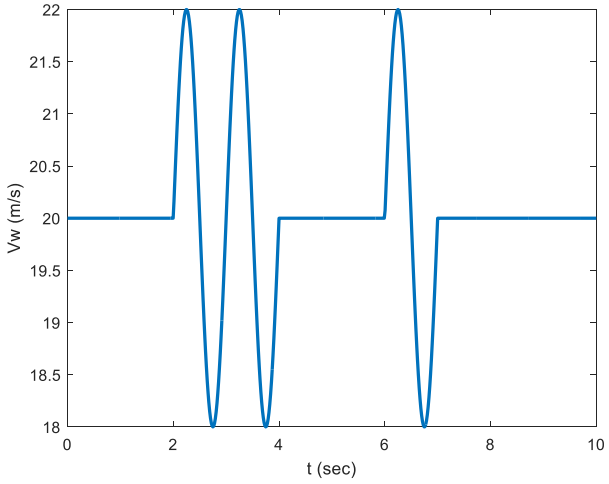

Fig. 18 Wind speed profile including the scenario of gusts

3.2. Discussion

For the ramp wind speed test, the WT goes through the first zone from 0 to 2 seconds. The electrical power profile shows that the WT is in its OFF mode with 0 Watts production since in this first zone the mechanical power in the wind is not sufficient to generate significant electrical power. Moreover, the angular speed is that low that physical variables such as torque and tip speed ratio are not defined.

The second zone is located between 2 and 4 seconds. Electrical power shows a growing tendency with the increasing wind speed. The power is under the maximum value, but it meets the optimal value that can be generated by the WT.

From 4 to 8.3s the wind speed goes from 12 to 25 m/s which falls within the third zone. The wind speed is strong enough to generate high values of the power that go beyond the rated maximum power of the machine. Therefore, the power is limited to its maximum value that can be seen through the curve at around 6.5 kW. The power falls to 0 W in the last zone as the wind is too strong, where the WT is put out of service.

The current results in Figure 10 show that the first control strategy allows the current to follow their references except in the second zone and more specifically around the transition between zone 1 and 2. The speed does not accurately follow its reference either in the second zone as can be observed in Figure 11. Figures 14 and 15 show how the proposed strategy improved the tracking performance for the currents and the angular speed offering better transitions between the zones.

The test of the WT under gusts effects is performed with the wind profile presented in Figure 18. The gusts are introduced at 2 and 6 seconds with 2 m/s amplitude and 1Hz of frequency, which is realistic considering real gusts that are usually located between 0.1 to 1 Hz. The electrical power curve presented in Figure 17 shows that power remains closely stable even with the presence of gusts showcasing the efficiency of the control strategies.

Although the proposed technique demonstrates promising performance and improved power quality and control signals, the study was conducted under certain limitations. These include residual peaks and disturbances during transitions between the wind turbine's operating zones, as well as under uncertain and varying wind conditions. Moreover, the proposed method has been evaluated only for a single wind turbine considering a specific type and rated power. The extension of the proposed technique to multi-turbine configurations in wind farms has not yet been investigated. Furthermore, the state feedback and back stepping methodologies reply on the model's parameters which needs more robust components to be included in the control strategy. Finally, the results are derived from MATLAB/Simulink simulations using realistic wind profiles. Experimental validation remains unexplored.

4. Conclusion

This work has examined the control of horizontal-axis wind turbines under challenging and variable conditions due to the presence of wind gusts in the wind speed tested profiles. The work highlights the critical role of the state feedback and Backstepping controllers in ensuring the achievement of the control objectives. By addressing the dynamic interaction between the turbine dynamics and control actions, the study demonstrates that effective gust mitigation can significantly maintain power extraction close to optimal levels in the second zone and maximal power in the third zone. The results underline the importance of the proposed improved control scheme that efficiently responded to transient wind events thanks to the polynomial interpolation technique. The SVPWM on the other hand contributed to delivering smoother control signals to the generator. These findings

are important as these scenarios are becoming increasingly relevant with the growth of turbines and their deployment in more complex atmospheric environments. Despite all contributions, several avenues for future research remain open. Future work may include further improvement of power quality in the transitions between the wind turbine's operating zones by integrating high-fidelity wind field estimation, perception-based and more robust techniques to enhance anticipated reactions and model parameters variations. Additionally, the development of data-driven and learning-based controllers might enhance adaptability under uncertain and varying wind conditions. Finally, extending the research effort to include multiple turbines cases in wind farms with experimental validation or field-scale testing would strengthen the practical applicability of the proposed approaches.

Acknowledgement
This research was not funded by any grant.

References

[1] Pincelli, Isabella Pimentel, Jim Hinkley, and Alan Brent. "Developing Offshore Wind Farms in Aotearoa New Zealand: An Analysis of Life Cycle Carbon Emissions, Materials and Energy Implications." Wind Energy 28, no. 4 (2025). https://doi.org/10.1002/we.70009

[2] Ruan, Ziwen, Xi Lu, Zihua Yin, et al. "Spatiotemporal Carbon Footprint and Associated Costs of Wind Power toward China's Carbon Neutrality." Resources, Conservation and Recycling 205 (2024): 107593. https://doi.org/10.1016/j.resconrec.2024.107593

[3] Pfadt-Trilling, A. R., and M.-O. P. Fortier. "Carbon Footprint and Energy Payback Time of a Micro Wind Turbine for Urban Decarbonization Planning." Scientific Reports 15, no. 1 (2025). https://doi.org/10.1038/s41598-025-10540-x

[4] Benbouhenni, Habib, Mourad Yessef, Ilhami Colak, et al. "Dynamic Performance of Rotor-Side Nonlinear Control Technique for Doubly-Fed Multi-Rotor Wind Energy Based on Improved Super-Twisting Algorithms under Variable Wind Speed." Scientific Reports 14, no. 1 (2024). https://doi.org/10.1038/s41598-024-55271-7

[5] Leza, Melkamu Bekele, Ayodeji Olalekan Salau, Milkias Berhanu Tuka, et al. "Optimization of DFIG Performance in Wind Energy Systems Using Fuzzy Logic Control and Harmonic Mitigation." Journal Européen Des Systèmes Automatisés 58, no. 7 (2025): 1525–35. https://doi.org/10.18280/jesa.580720

[6] Amrane, Fayssal, and Hichem Itouchene. "Enhanced Fuzzy-Power Control for WECS Based on Variable Wind Speed-Driven DFIG Using SVM Strategy under Sub- and Super-Synchronous Operating Modes." Periodica Polytechnica Electrical Engineering and Computer Science 69, no. 3 (2025): 215–25. https://doi.org/10.3311/ppee.39807

[7] Ramadan, Aya Hamdy, Mahmoud A. Attia, S. F. Mekhamer, et al. "Advanced Control Strategies for Wind Turbine Blade Angle Systems: A Comparative Study of Optimization Algorithms and Controllers." International Journal of Energy Research 2025, no. 1 (2025). https://doi.org/10.1155/er/5550970

[8] Fu, Deyi, Shiyao Qin, Lingxing Kong, Yang Xue, Lice Gong, and Anqing Wang. "Wind Turbine Load Optimization Control and Verification Based on Wind Speed Estimator with Time Series Broad Learning System Method." IET Control Theory & Applications 18, no. 17 (2024): 2215–27. https://doi.org/10.1049/cth2.12635

[9] Zhang, Bowen, Wei Luo, Zhaohui Luo, Jian Xu, and Longyan Wang. "Effectiveness of Wake Control Optimization for Multiple In-Line Wind Turbines by Combinatorial Machine Learning Wake Model." Proceedings of the Institution of Mechanical Engineers, Part C: Journal of Mechanical Engineering Science 238, no. 5 (2023): 1280–94. https://doi.org/10.1177/09544062231185516

[10] Wei, Bo, Hao Hu, and Shuangao Wang. "Coordinated Power and Mechanical Loads Optimization Strategy of Wind Turbine Based on Model Predictive Control." Journal of Control, Automation and Electrical Systems 36, no. 4 (2025): 636–47. https://doi.org/10.1007/s40313-025-01182-5

[11] Tang, Minan, Wenjuan Wang, Yaguang Yan, Yaqi Zhang, and Bo An. "Robust Model Predictive Control of Wind Turbines Based on Bayesian Parameter Self-Optimization." Frontiers in Energy Research 11 (2023). https://doi.org/10.3389/fenrg.2023.1306167

[12] Zhang, Zhiyuan, Bo Jiao, Haihua Lin, Chengmeng Sun, Hongyuan Sun, and Yoo Sang Choo. "Blade Pitch Control Strategy for Floating Wind Turbines Based on Fractional Order PIDD2." Journal of Marine Science and Application, ahead of print, January 14, 2026. https://doi.org/10.1007/s11804-026-00846-1

[13] Ait-Chekdhidh, Zaina, Aghiles Ardjal, and Maamar Bettayeb. "Fractional Order Sliding Mode Control Based Funnel Control of Wind Turbine for Maximum Power Point Tracking." Proceedings of the Institution of Mechanical

Engineers, Part A: Journal of Power and Energy 239, no. 7 (2025): 1103–18. https://doi.org/10.1177/09576509251375508

[14] Kadi, Sara, Habib Benbouhenni, Adil Yahdou, et al. “Performance Optimization of Wind Turbines via Fractional-Order Type 2 Fuzzy MPPT Control.” Measurement and Control, ahead of print, December 10, 2025. https://doi.org/10.1177/00202940251398969

[15] Leulmi, Mohammed Islam, Samir Ladaci, and Horst Schulte. “A Novel State–Space Model Reference Adaptive Speed Control Design for Fractional-Order Model-Based Wind Turbine.” International Journal of Electrical Power & Energy Systems 170 (2025): 110599. https://doi.org/10.1016/j.ijepes.2025.110599

[16] Pompodakis, Evangelos, Arif Ahmed, Georgios Orfanoudakis, and Dimitris Katsaprakakis. “A MILP Optimization Approach for Optimizing Primary Frequency Control of Wind Turbines in Low-Inertia Islands.” Wind Energy and Engineering Research 5 (2026): 100024. https://doi.org/10.1016/j.weer.2026.100024

[17] Tessaro, Heitor José, and Ricardo Vasques Oliveira. “Operating Point Optimization of Wind Turbine Generators for Provision of Inertial Response and Frequency Control.” International Transactions on Electrical Energy Systems 30, no. 6 (2020). https://doi.org/10.1002/2050-7038.12382

[18] Fu, Deyi, Lingxing Kong, Lice Gong, Anqing Wang, Haikun Jia, and Na Zhao. “Wind Turbine Load Optimization Control Strategy Based on LIDAR Feed-Forward Control for Primary Frequency Modulation Process with Pitch Angle Reservation.” Energies 16, no. 1 (2023): 510. https://doi.org/10.3390/en16010510

[19] Hou, Chien Lun, Wei Yu, Mao Hsiung Chiang, and Po Wen Cheng. “Stochastic Model Predictive Control of a 10-MW Semi-Submersible Floating Offshore Wind Turbine: A Comparative Study with Gain-Scheduled PI, LQR and MPC Controllers.” Ocean Engineering 340 (2025): 122431. https://doi.org/10.1016/j.oceaneng.2025.122431

[20] Ma, Junchao, Jianing Liu, Zhen He, et al. “Probabilistic Assessment Method of Available Inertia for Wind Turbines Considering Rotational Speed Randomness.” Energies 18, no. 24 (2025): 6457. https://doi.org/10.3390/en18246457.

[21] Zhang, Chuanzhi, Yijing Chen, Dawei Zhao, Chunhua Li, Xiaojiang Guo, and Jing Bu. “Individual Pitch Control for Load Reduction of Offshore Wind Turbine Based on Particle Swarm Optimization and Fuzzy Logic.” IET Renewable Power Generation 19, no. 1 (2025). https://doi.org/10.1049/rpg2.70000

[22] Eskandari, Ahmadreza, and Ramin Vatankhah. “Opposition-Based Particle Swarm Optimization-Aided Neural Fractional Order PID Pitch Control for Variable Pitch Wind Turbines.” International Journal of Dynamics and Control 13, no. 6 (2025). https://doi.org/10.1007/s40435-025-01703-9

[23] Astolfi, Davide, Francesco Castellani, and Francesco Natili. “Wind Turbine Yaw Control Optimization and Its Impact on Performance.” Machines 7, no. 2 (2019): 41. https://doi.org/10.3390/machines7020041

[24] Zhang, Ziyu, Peng Huang, Girma Bitsuamlak, and Shuyang Cao. “Analytical Solutions for Yawed Wind-Turbine Wakes with Application to Wind-Farm Power Optimization by Active Yaw Control.” Ocean Engineering 304 (2024): 117691. https://doi.org/10.1016/j.oceaneng.2024.117691

[25] Astolfi, Davide, Francesco Castellani, and Francesco Natili. “Data-Driven Methods for the Analysis of Wind Turbine Yaw Control Optimization.” Journal of Solar Energy Engineering 143, no. 1 (2020). https://doi.org/10.1115/1.4047413

[26] Alwash, Saad M., Osama Qasim Jumah Al-Thahab, and Shamam F. Alwash. “Modeling and Control Strategies for DFIG in Wind Turbines: A Comparative Analysis of SPWM, THIPWM, and SVPWM Techniques.” Journal Européen Des Systèmes Automatisés 56, no. 6 (2023): 963–72. https://doi.org/10.18280/jesa.560607

[27] Tawfiq, Kotb B., Peter Sergeant, and Arafa S. Mansour. “Comparative Analysis of Space Vector Pulse-Width Modulation Techniques of Three-Phase Inverter to Minimize Common Mode Voltage and/or Switching Losses.” Mathematics 12, no. 18 (2024): 2832. https://doi.org/10.3390/math12182832

[28] Boukadoum, A., A. Bouguerne, and T. Bahi. “Direct Power Control Using Space Vector Modulation Strategy Control for Wind Energy Conversion System Using Three-Phase Matrix Converter.” Electrical Engineering & Electromechanics, no. 3 (2023): 40–46. https://doi.org/10.20998/2074-272x.2023.3.06

[29] Lin, Zifan, Xinan Zhang, Jianguo Zhu, Wenxiang Du, Jiahan Ye, and Yang Bai. “Advances in Space Vector Modulation Techniques for Multilevel Inverters: A Comprehensive Review.” Chinese Journal of Electrical Engineering 11, no. 2 (2025): 63–77. https://doi.org/10.23919/cjee.2025.000146

[30] Jayakumar, Vinoth, Bharatiraja Chokkalingam, and Josiah Lange Munda. “A Comprehensive Review on Space Vector Modulation Techniques for Neutral Point Clamped Multi-Level Inverters.” IEEE Access 9 (2021): 112104–44. https://doi.org/10.1109/access.2021.3100346

[31] Abubakar, Muhammad Nazir, F.W. Burari F.W. Burari, and O.W. Olasoji O.W. Olasoji. “Modeling and Control of Wind Turbines.” International Journal of Advances in Engineering and Management 7, no. 8 (2025): 839–48. https://doi.org/10.35629/5252-0708839848

[32] Shalbafian, Arefe, Farhad Amiri, and Soheil Ganjefar. "Adaptive Robust Nonlinear Optimal Sliding Mode Control for Wind Turbines: A Hybrid OHAM-Based Approach to Maximize Power Capture." IET Renewable Power Generation 19, no. 1 (2025). https://doi.org/10.1049/rpg2.70131

[33] Ibrahim, Luay G., and Salam Waley Shneen. "Study and Analysis of Adaptive PI Control for Pitch Angle on Wind Turbine System." International Journal of Robotics and Control Systems 5, no. 2 (2025): 1331–47. https://doi.org/10.31763/ijrcs.v5i2.1850.

[34] Shanto, Md Atiqur Rahaman, Md Mokaddes Hossain Tonmoy, Md Nahid Islam, Azam Jaman, and Ifte Khairul Amin. "Modeling and Control Strategy of PMSG-Based Ocean Wave Energy Conversion Systems." Transactions of the Indian National Academy of Engineering 10, no. 2 (2025): 433–51. https://doi.org/10.1007/s41403-025-00527-5

[35] Bijarani, Muhammad Ali, Ghulam Sarwar Kaloi, Zohaib Hussain Leghari, Mohammad R. Altimania, Hafiz Mudassir Munir, and Ievgen Zaitsev. "Lyapunov Stability Scheme Based Nonlinear Power Transfer Matrix Model for Power Control and Modeling of PMSG-Wind Turbines." Energy Science & Engineering 14, no. 1 (2025): 364–76. https://doi.org/10.1002/ese3.70361

[36] Zioui, Nadjet, Aicha Mahmoudi, Mehdi Fazilat, Oumar Kone, Reda Dermouche, and Mohamed Tadjine. "Quantum Space Vector Pulse Width Modulation for Speed Control of Permanent Magnet Synchronous Machines." E-Prime - Advances in Electrical Engineering, Electronics and Energy 13 (2025): 101074. https://doi.org/10.1016/j.prime.2025.101074

[37] Majout, Btissam, Badre Bossoufi, Mohammed Karim, et al. "Artificial Neural Network-Based Direct Power Control to Enhance the Performance of a PMSG-Wind Energy Conversion System under Real Wind Speed and Parameter Uncertainties: An Experimental Validation." Energy Reports 11 (2024): 4356–78. https://doi.org/10.1016/j.egyr.2024.03.039